Grain size and sample size interact to determine strength in a soft metal

Bruno Ehrler, Xiaodong Hou, Tingting Zhu, Ken M y P'Ng, Chris J Walker, Andy Bushby, David James Dunstan

Grain size and sample size interact to determine strength in a soft metal

Journal:	*Philosophical Magazine & Philosophical Magazine Letters*
Manuscript ID:	TPHM-08-Apr-0106.R2
Journal Selection:	Philosophical Magazine
Date Submitted by the Author:	04-Aug-2008
Complete List of Authors:	Ehrler, Bruno; Queen Mary University of London, Physics Hou, Xiaodong; Queen Mary University of London, Materials Zhu, Tingting; Queen Mary University of London, Materials P'ng, Ken; Queen Mary University of London, Materials Department Walker, Chris; Queen Mary, University of London, Physics Bushby, Andy; Queen Mary, University of London, Materials Dunstan, David; Queen Mary University of London, Physics
Keywords:	micromechanics, plastic deformation, plasticity of metals, work-hardening
Keywords (user supplied):	micromechanics, plastic deformation, plasticity of metals

Grain size and sample size interact to determine strength in a soft metal

B. Ehrler,* X.D. Hou,† T.T. Zhu,† K.M.Y. P'ng,†
C.J. Walker,* A.J. Bushby† and D.J. Dunstan*

Centre for Materials Research,
Queen Mary, University of London,
London E1 4NS, England.

* Department of Physics
† Department of Materials, School of Engineering and Materials Science

PACS: 62.20.Fe, 46.35.+z, 81.05.Bx

Keywords: Plastic yield, Size effect, Grain size, Soft metal

Corresponding Author:
David J Dunstan, Dept of Physics, Queen Mary, University of London, London E1 4NS
Tel. 020 7882 3687, Fax 020 8981 9465, e-mail d.dunstan@qmul.ac.uk

Other Authors

Bruno Ehrler, Dept of Physics, Queen Mary, University of London, London E1 4NS
Tel. 020 7882 5050, Fax 020 8981 9465, e-mail bruno.ehrler@gmx.de

Xiaodong Hou, Dept. of Materials, Queen Mary, University of London, London E1 4NS
Tel. 020 7882 3687, Fax 020 8981 9804, e-mail x.hou@qmul.ac.uk

Tingting Zhu, Department of Materials, Queen Mary, University of London, London E1 4NS
Tel. 020 7882 3687, Fax 020 8981 9804, e-mail x.hou@qmul.ac.uk

Ken M.Y. P'ng, Dept of Materials, Queen Mary, University of London, London E1 4NS
Tel 020 7882 3762, Fax 020 8981 9804, e-mail m.y.png@qmul.ac.uk

Chris J. Walker, Dept of Physics, Queen Mary, University of London, London E1 4NS
Tel. 020 7882 5050, Fax 020 8981 9465, e-mail c.j.walker@qmul.ac.uk

Andrew J. Bushby, Dept of Materials, Queen Mary, University of London, London E1 4NS
Tel. 020 7882 5276, Fax 020 8981 9804, e-mail a.j.bushby@qmul.ac.uk

Abstract: Understanding the strengthening of small-scale materials and structures is one of the key issues in nanotechnology. Many theories exist, each addressing a small domain of experimentally observed size effects and invoking different mechanisms. Measurements of the stress-strain relationship of nickel foils in flexure by the load-unload method provide strikingly accurate data from the elastic region through the yield point and to high plastic strain. The data shows that the effects on the rate of work-hardening due to crystallite size and sample size interact, while in existing theories they should be independent. Existing theories cannot be complete. The symmetry of the dependence of flow stress on grain size and structure size suggests that strengthening effects are due to a finite strained volume however this is delimited.

1. Introduction

A key aspect of nanotechnology is the effect of small-scale phenomena on the mechanics of materials. A wide variety of size effects have been reported over the years in the strength of small structures, microstructured materials, and in materials under localised loading leading to high strain gradients. The size effect in brittle materials is described by the classic Griffith's theory of cracking [1]. The concept of critical thickness for a uniformly strained epitaxial crystal layer, in which the yield stress follows an inverse dependence on the thickness h, was proposed initially for metals in 1949 [2], and the theory has been developed since then primarily for semiconductors [3,4]. In the Hall-Petch effect, the flow stress of a metal follows accurately a dependence on the inverse square root of the crystallite (grain) size d. It has been known since 1951 [5,6], and rather naturally attributed to interactions between dislocations and grain boundaries. It is most directly observed in the yield stress or the flow stress at small plastic strain, but many authors also report that the work-hardening rate shows the same inverse square-root dependence on the grain size. Strain-gradient plasticity was identified much more recently. In this phenomenon, a term in the plastic strain gradient is added to the expression for the flow stress. It is considered to arise from the geometrically necessary dislocations that have to be present if there is to be a plastic strain gradient. The best experimental evidence for it comes from measurements of the stress-strain relationship for thin copper wires in torsion [7] and for thin nickel foils in flexure (bending) [8]. However, these reported experimental results do not cover a sufficient range of strains and grain sizes. In this paper, we extend the foil flexure method of Stölken and Evans [8] to a range of nickel foils with grain sizes d extending from less than the foil thickness h to more than h, and to a range of strains from below yield to values near 0.1, to obtain data orders of magnitude better than previous data in both accuracy and range.

Although Armstrong identified the coexistence of a structure size effect with the grain size effect [9], the Hall-Petch effect has not been systematically studied in small structures (i.e. structures with a characteristic length $h \sim d$). Venkateswaran and Bravman studied aluminium films on silicon substrates and obtained the flow stress and its dependence on film thickness [10]. However, they had only two grain sizes and were not able to distinguish between the Hall-Petch $d^{-½}$ dependence and the d^{-1} dependence that they considered more plausible. They assumed that the effects of h and d are separable. Thompson explained their results using critical thickness theory (and introducing a critical grain size as well as a critical thickness) but the theory necessarily yields a d^{-1} dependence rather than the Hall-Petch $d^{-½}$ [11]. Other than this, critical thickness effects have not been studied as a function of grain size. Strain-gradient plasticity has not been studied through the yield point, nor as a function of grain size. Mechanistic explanations or theoretical explanations for these effects do not consider interaction between them.

In this paper, we report data for thin nickel foils with a range of grain sizes, so that h and d are both varied in the crucial range of tens of microns. Using bending techniques, data was obtained from the elastic regime through the yield stress to plastic strains of nearly 10%. The effect of critical thickness on the yield stress and also the classic Hall-Petch effect on the yield stress are both clearly seen. However, in the plastic regime, our data show that the strain-gradient or critical thickness effects and the Hall-Petch effect on the work-hardening and the flow stress are intimately linked. This linkage has not been explored in strain-gradient plasticity theory. It requires a reconsideration of the mechanisms both of the Hall-Petch effect and of strain gradient plasticity. Recently, remarkably high compressive yield strengths have been reported in small nickel [12,13] and gold pillars [14,15]. Volkert and Lilleodden [15] found that the yield strengths of gold micro-pillars varied approximately with the inverse square-root of the pillar diameter a. Taken together with these data, our results imply that all

the size effects could be unified into a single size effect in which a small stressed volume is stronger than bulk material however the small volume is delimited. However, a theory of a single size effect remains to be established.

2. Stress-Strain Experiments

Stress-strain data around the yield point of soft metals is notoriously hard to obtain, yet is crucial for developing an understanding the data at higher strain. We use the load-unload technique familiar in materials testing, but introduced in the present context of the flexural strength of thin metal foils by Stölken and Evans [8]. A foil of thickness h and width w is wrapped round a mandrel or former of known radius R_1 (Fig. 1) giving a surface strain, $\varepsilon_S = ½\ h/R_1$. This introduces a known strain, which is partly elastic and partly plastic. The foil is then unloaded, and it relaxes elastically to a larger radius of curvature R_2 (Fig.1) with a reduced surface strain $\varepsilon_S = ½\ h/R_2$. The increase in radius provides a determination of the bending moment M at the radius R_1. At the radius R_2 the bending moment is zero. At the radius R_1 simple elastic beam theory gives, for the bending moment normalised by wh^2,

$$M_n = \frac{M}{wh^2} = \frac{Eh}{12}\left(\frac{1}{R_1} - \frac{1}{R_2}\right) = \frac{E}{6}\Delta\varepsilon_S \qquad (1)$$

where $E = c_{11} - c_{12}^2 / c_{11} = Y/(1-\nu^2)$ is the relevant elastic modulus for a wide beam where the lateral strain is zero, and for nickel, the Young's modulus Y = 200 GPa, the Poisson's ratio ν = 0.31 giving E = 220 GPa.

Fig.1 around here

With a suitable range of formers and mandrels and using non-contact optical profilometry to measure curvatures, the load-unload technique can give excellent data over a very wide range of surface strain. A single foil is used to generate a stress-strain curve, by starting with the largest radius of curvature and carrying out the load-unload sequence of

measurements on progressively smaller radii of curvature. When the foil is deformed plastically, subsequent elastic relaxation leaves residual stresses in the beam, and puts the surfaces into the opposite state of stress. Consequently, we use not the surface stress but the normalised bending moment M_n for plotting against the surface strain $\varepsilon_S = ½\ h/R_1$, as these two quantities are directly obtained from the raw data, and they are readily fitted with theoretical curves. The normalised bending moment has units of pressure (Pa) and we therefore refer to it in what follows as the 'bending stress'.

Nickel foils having three thicknesses (h = 10, 50 and 125 μm) of purity 99.95%, 99.90% and 99.99%, respectively, were obtained commercially (Goodfellows Ltd., Cambridge, UK). For each foil, three different grain sizes were attained by rapid thermal annealing under vacuum. Although it was not possible to choose annealing conditions that would generate the same grain sizes, d, for each foil thickness, it was feasible to obtain d ~ 30 μm at each thickness. As described by Moreau *et al.* [16], after etching of the grain boundaries (in a mixture of acetic and nitric acid for about two minutes), the grain size was measured by optical microscopy. Additionally, the microstructure of the cross section was characterized in a scanning electron microscope (Carl Zeiss Supra-40 FEGSEM) by electron backscattered diffraction (EBSD, HKL5, Oxford Instruments, UK). The grains are equiaxed. The grain sizes measured by EBSD and by the surface etch technique are consistent. The pole figures obtained by EBSD indicate a random texture. More details are given in the supplementary on-line material.

This set of specimens gave nine sets of data for bending stress against surface strain; all nine datasets are tabulated in the supplementary on-line material. Figure 2 shows the data for foils of thicknesses h = 10μm, 50μm and 125μm, and of grain size d about 30μm in all three foils, in log-log form to cover the large range of strain from about 10^{-5} to 10^{-1}. The inset

in Fig.2 is a linear plot to show the elastic-plastic transition in more detail. For comparison, the earlier data reported by Stölken and Evans [8] are also shown.

Fig.2 near here

We fit these data using classical plasticity theory (solid lines in Fig.2), with linear work-hardening, using

$$\begin{aligned} \sigma(\varepsilon) &= E\varepsilon \qquad \sigma \le \sigma_0 \\ \sigma(\varepsilon) &= \sigma_0 + k\varepsilon_p \quad \sigma \ge \sigma_0 \end{aligned} \tag{2}$$

where σ_0 is the yield stress (in tension and in compression: we assume the material behaves identically), k is the rate of linear work hardening, and $\varepsilon_p = \varepsilon - \sigma_0/E$ is used as a close approximation (for k << E) to the true plastic strain, $\varepsilon - \sigma(\varepsilon)/E$. In classical plasticity theory, plastic yield occurs when the stress reaches the yield stress. The beam is deformed elastically from the centre, $z = 0$, to $z = \pm z_0$ where z_0 is defined by $Ez_0 / R_1 = \sigma_0$. From $\pm z_0$ to the free surfaces at $z = \pm$ ½h the deformation is plastic. This gives the following expression for the bending stress when plasticity occurs,

$$\begin{aligned} M_n &= \frac{1}{h^2}\int_{-½h/2}^{½h/2} z\sigma(\varepsilon)dz = \frac{2}{h^2}\int_0^{z_0}\frac{z^2E}{R_1}dz + \frac{2}{h^2}\int_{z_0}^{h/2} z\left(\sigma_0 + k\frac{(z-z_0)}{R_1}\right)dz \\ &= \left(\frac{\sigma_0}{4} - \frac{\sigma_0^3}{12E^2\varepsilon_S^2}\right)\left(1-\frac{k}{E}\right) + \frac{k\varepsilon_S}{6} \end{aligned} \tag{3}$$

and this is the function fitted to our data in Fig.2. Linear work hardening is adequate to describe the data as can be seen from Fig. 2 at large strains. Close inspection around the yield point (Fig.2 inset) shows that the onset of yield is more complicated than the model assumes. There can be some plastic yield at as little as half the bending stress corresponding to σ_0. In what follows, therefore, we refer to σ_0 as the 'fitted yield stress' – this can be considered to represent the onset of gross plasticity.

Fig.3 near here

It is clear from Figs 3 and 4(a) that both σ_0 and k depend upon both d and h, increasing as the grain size and foil thickness are decreased. Traditionally these are separate effects [9, 10, 11]. The data in Fig.3 for σ_0 are consistent with this. The fitted yield stress data agree with

$$\sigma_0(d,h) = \frac{330}{\sqrt{d}} + \frac{430}{h} = \frac{\sigma'_{HP}}{\sqrt{d}} + \frac{\sigma'_{CTT}}{h} \qquad (4)$$

with σ_0 in MPa and d and h in microns (solid lines in Fig 3), that is, additive effects for h and d, and – perhaps surprisingly – with no breakpoint between $d<h$ and $d>h$. The first term may be interpreted as the Hall-Petch effect (the inverse square root of grain-size) [5,6] with the constant $\sigma'_{HP} = 0.33$ MPa m^{½}, independent of foil thickness. Values of σ'_{HP} for bulk nickel from 0.16 to 0.45 MPa m^{½} have been reported [17,18]. Our value is in this range, in accordance with the classical Hall-Petch behaviour at the yield point. The second term is an additive term $\sigma_{CTT} = \sigma'_{CTT} h^{-1}$ for the critical thickness effect which increases the yield stress in the thinner foils, independent of grain size [19]. The critical thickness term has been previously observed by Moreau *et al* [15], and the full theory was given in Ref.19. It is particularly interesting that the natural size for critical thickness theory in beam-bending is not the beam thickness h itself, but the thickness h_{plast} within which critical thickness theory predicts plasticity is initiated. A characteristic length in critical thickness theory may be defined as $L_C = bE/\sigma_0 = b/\varepsilon_0$ where b is the Burgers vector and ε_0 is the bulk yield strain. Then $h_{plast} = L_C\left(-1+\sqrt{1+h/L_C}\right)$ [19]. This is approximately 2 μm in our 10 μm foils and approximately 8 μm in our 125 μm foils.

Fig.4 near here

In contrast to the yield-point data, in the work-hardening data in Fig.4(a) for k, the effects of d and h are apparently multiplicative. The work-hardening data fit well to

$$k(d,h) = \frac{120}{\sqrt{d}\sqrt{h}} \qquad (5)$$

with k in GPa and d and h in microns. Normalising by multiplying by $\sqrt{h}$, the nine data points fall on a single straight line (Fig.4(b)). From the data of Stölken and Evans [8] we can estimate very approximately k values of 1 GPa for their 50 μm foil with 71 μm grain size, and 2.5 GPa for their 12.5 μm foil with 31 μm grain size. Our equivalent k values, from eq.5, are 2 GPa and 6 GPa respectively, consistent within their error bars.

Other fits are possible. For example, a square-root work-hardening law might be used at small plastic strains instead of the linear work-hardening of Eqn.2. This would fit the data around the elbow in Fig.2 more accurately and it would yield different values for the fitted yield point σ_0. Going further, one may be sceptical of the physical meaning of a yield stress in a soft metal. What is observed may be interpreted not as a yield stress but merely as the flow stress at the lowest resolved plastic strain. Then it may be more instructive to plot the raw data differently. We follow Thompson [11] in supposing that the flow stress should depend upon grain size and structure size as $d^{-1} + h^{-1}$. Figure 5 shows a log-log plot of bending moment at a wide range of strains against an effective length or size ℓ_{eff} given by $\ell_{\text{eff}}^{-1} = d^{-1} + h^{-1}$. At all strains, the data are consistent with straight-line fits. However, at low strains the gradients are very close to –½, indicating a Hall-Petch like dependence on the effective size ℓ_{eff}. At high strains, the gradients are very close to –1 as in Thompson's theory [11]. This is interesting, as Thompson's theory would be expected to be valid at small plastic strains rather than at high. Their theory certainly does not predict the power $\ell_{\text{eff}}^{-1/2}$ observed here at small strains. However, these results are perhaps consistent with the approach of Narutani and Takamura [20] and others if the geometrically necessary dislocation density is to be added to the normal dislocation density.

Fig.5 near here

3. Discussion

No existing theories predict the totality of the results we report here. Indeed, a comprehensive and accurate data set such as we report here (and make available to other workers as on-line supplementary material) puts much higher constraints on any theoretical explanation of strength in small volumes than the data sets that theories have previously been confronted with. Nevertheless, it seems that still better data around the yield point would be desirable.

It does seem worth emphasizing the following point. Studies of grain size in bulk materials have finite d and infinite h (letting h be proxy for structure size or the characteristic length of a strain gradient), with d delimited by grain boundaries, and show very clearly the Hall-Petch $d^{-½}$ behaviour. The pillar-crushing experiments have finite h and infinite d (or $d = h$, depending how one conceptualises a finite single-crystal structure), with h delimited by free surfaces. They show clearly the $h^{-½}$ behaviour. The foil-bending experiments reported here have finite d and finite h, with d delimited by grain boundaries and h delimited by a free surface and by a strain gradient. The very clear symmetry shown between d and h in Eqn.5 and in Fig.5, and the absence of any breakpoint in the data or the fits between $d < h$ and $d > h$, suggest that these different ways of delimiting a finite volume or thickness have the same effect on the strength. That is, although we have no model to propose to explain these results, the data suggest that the size effect is driven by the finite strained volume, *whether* the strained volume is delimited by grain boundaries as in the classic Hall-Petch effect *or* by free surfaces as in the gold pillar experiments *or* by the finite volume set up by a strain gradient.

Acknowledgements

We are grateful to Dr W.J. Clegg and Prof. A Kelly (Cambridge), to Prof. A.G. Evans (University of California Santa Barbara) and to Dr N.M. Jennett (NPL) for valuable discussions, to Mr G. Gannaway (QMUL) for the construction of the equipment required for the bend tests, and to EPSRC for financial support.

References

1. A.A. Griffith, Phil. Trans. Roy. Soc. Lon. A**221**, 163 (1921)
2. F.C. Frank and J.H. van der Merwe, Proc. Roy. Soc. A**198**, 216 (1949).
3. J.W. Matthews and A.E. Blakeslee, J. Crystal Growth **27**, 118 (1974).
4. D.J. Dunstan, J. Mat. Sci.: Materials in Electronics **8**, 337 (1997).
5. E.O. Hall, Proc. Phys. Soc. Lon. B**64**, 747 (1951).
6. N.J. Petch, J. Iron Steel Inst. **174**, 25 (1953).
7. N.A. Fleck, G.M. Muller, M.F. Ashby and J.W. Hutchinson, Acta Metall. Mater. **42**, 475 (1994).
8. J.S. Stölken and A.G. Evans, Acta Mater. **46**, 5109 (1998).
9. R.W. Armstrong, J. Mech. Phys. Solids **9**, 196 (1961).
10. R. Venkatraman and J.C. Bravman, J. Mater. Res. **7**, 2040 (1992).
11. C.V. Thompson, J. Mater. Res. **7**, 237 (1993).
12. M.D. Uchic, D.M. Dimiduk, J.N.Florando and W.D. Nix, Science **305**, 986 (2004).
13. D.M. Dimiduk, M.D. Uchic and T.A. Parthasarathy, Acta Mater. **53,** 4065 (2005).
14. J.R. Greer, W.C. Oliver and W.D. Nix, Acta. Mater. **53**, 1821 (2005).
15. C.A. Volkert and E.T. Lilleodden, Philos. Mag. **86**, 5567 (2006).
16. P. Moreau, M. Raulic, K.M.Y. P'ng, G. Gannaway, P. Anderson, W.P. Gillin, A.J. Bushby and D.J. Dunstan, Phil. Mag. Lett. **85**, 339 (2005).
17. F. Ebrahimi, G.R. Bourne, M.S. Kelly and T.E. Matthews, Nanostruct. Mater. **11**, 343 (1999).
18. N. Hansen, Scripta Mater. **51**, 801 (2004).
19. D.J. Dunstan and A.J. Bushby, Proc. Roy. Soc. A**460**, 2781 (2004).
20. T. Narutani and J. Takamura, Acta Met. **39**, 2037 (1991).

Figure Captions:

Fig.1: Schematic of the load-unload method. The solid line represents the foil loaded to conform to the mandrel or former; the dotted line represents the foil after elastic recovery to the unloaded state.

Fig.2: The data are plotted as normalised bending stress $M_n = M / wh^2$ against surface strain ε_S over the full range of our experiments, for the foil thicknesses (i) 10 μm ■, (ii) 50 μm ● and (iii) 125 μm ▲. Grain sizes are approximately 30 μm in all three foils. The data of Stölken and Evans[8] is shown with their error bars (┼). In the inset (linear scale) the region at low strain is shown in more detail. The solid curves are fits using classical plasticity theory, eq.3, with the two fitting parameters σ_0 and k.

Fig.3: The fitted yield stress σ_0 is plotted against the inverse square root of the grain size for the three foil thicknesses ■10 μm, ● 50 μm, and ▲125 μm. The solid curves are the fits of eq.4.

Fig.4: In (a), the work-hardening parameter k is plotted against the inverse square root of the grain size, for the three thicknesses ■10 μm, ● 50 μm, and ▲125 μm. The solid curves are the fits of eq.5. In (b), the work-hardening parameter is normalised by multiplying by $\sqrt{h}$ and the solid line is a fit to the data for all three foil thicknesses.

Fig.5: The data for the bending stress at three different values of strain and all nine combinations of grain size d and foil thickness h are plotted against the effective size defined

by $\ell_{\text{eff}}^{-1} = d^{-1} + h^{-1}$. On the double logarithmic plot the data show little scatter and are consistent with slopes varying from –½ at low strain to –1 at high strain.

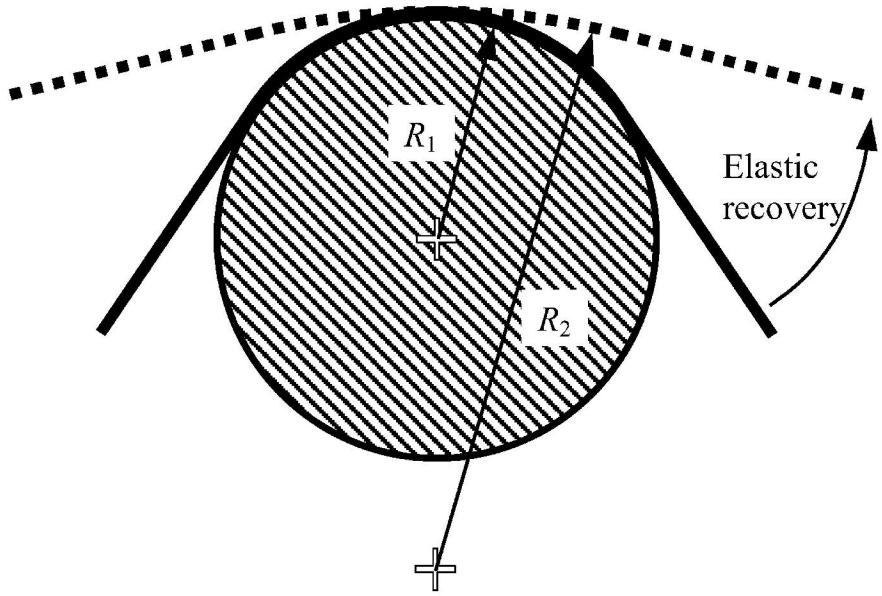

Figure 1
159x106mm (600 x 600 DPI)

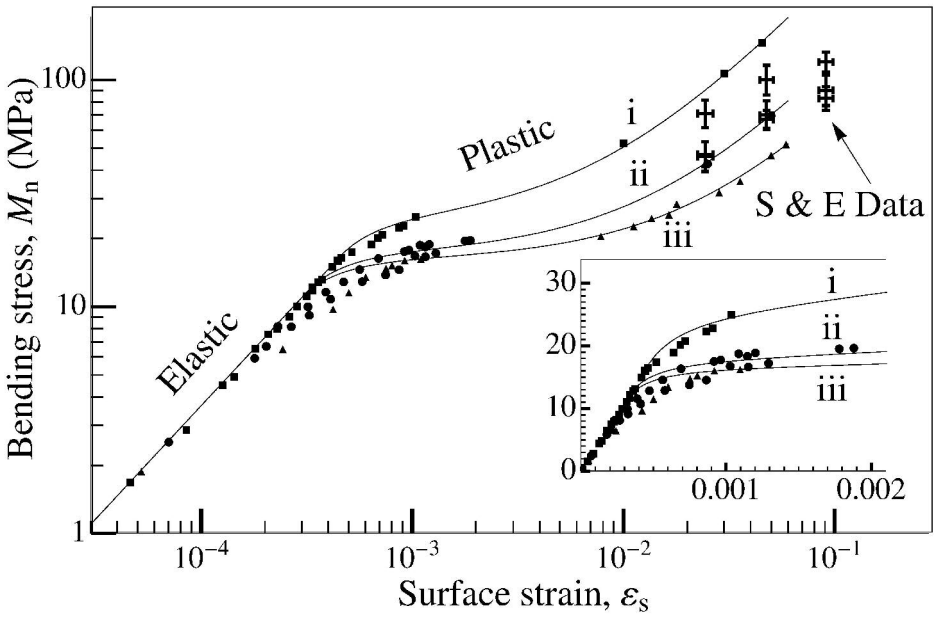

Figure 2
228x149mm (600 x 600 DPI)

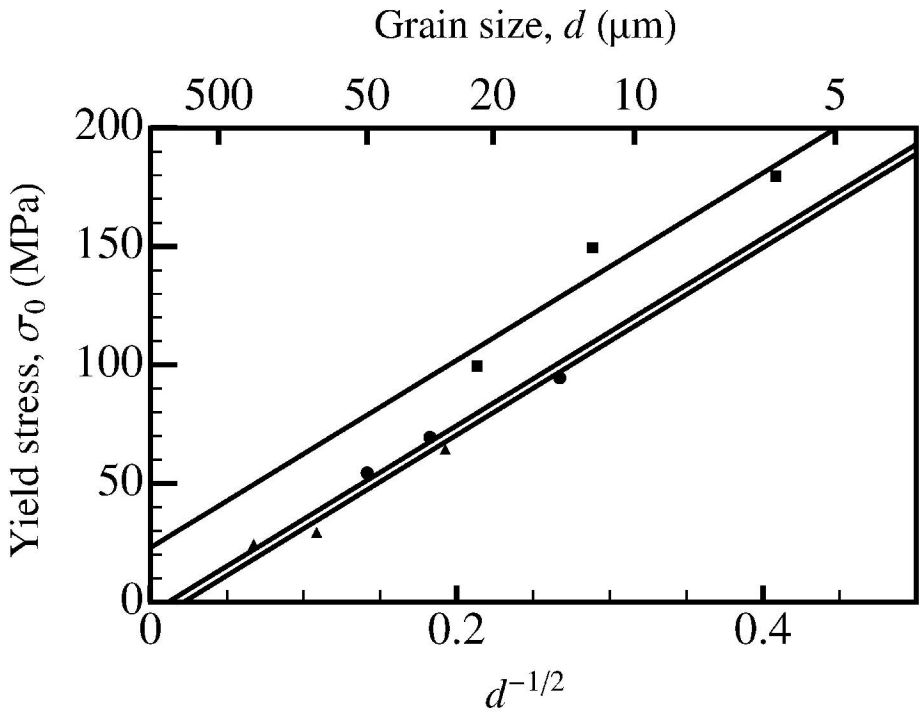

Figure 3
152x117mm (600 x 600 DPI)

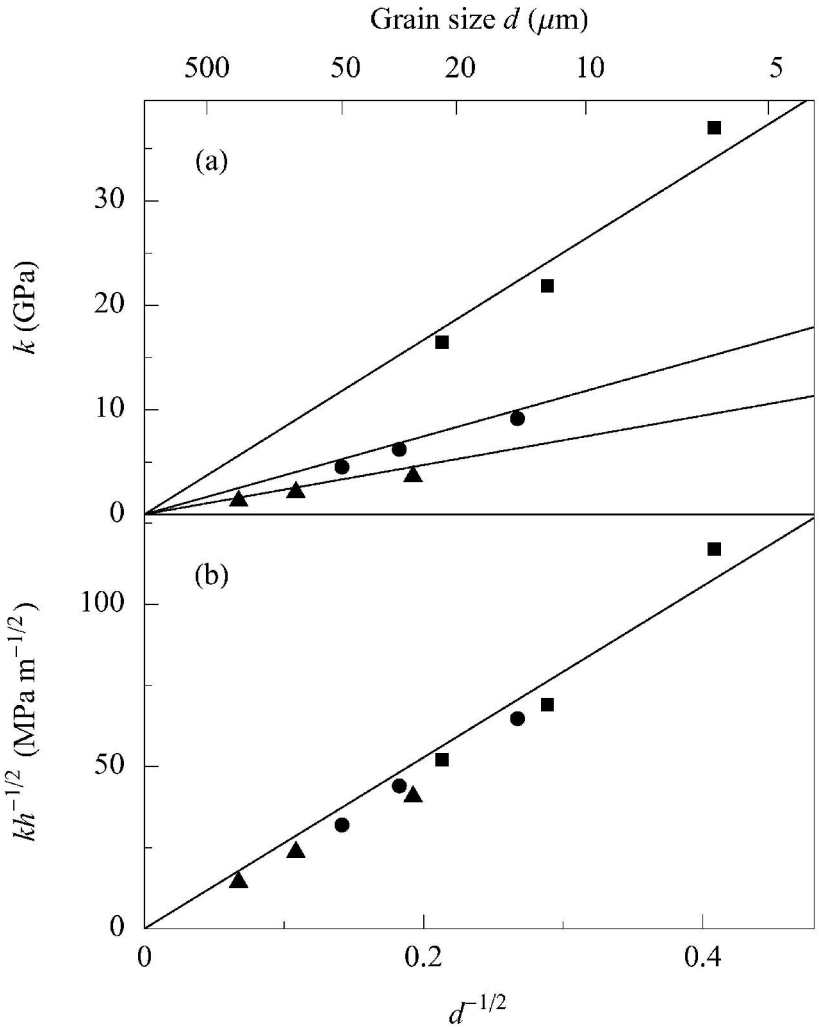

Figure 4
114x127mm (600 x 600 DPI)

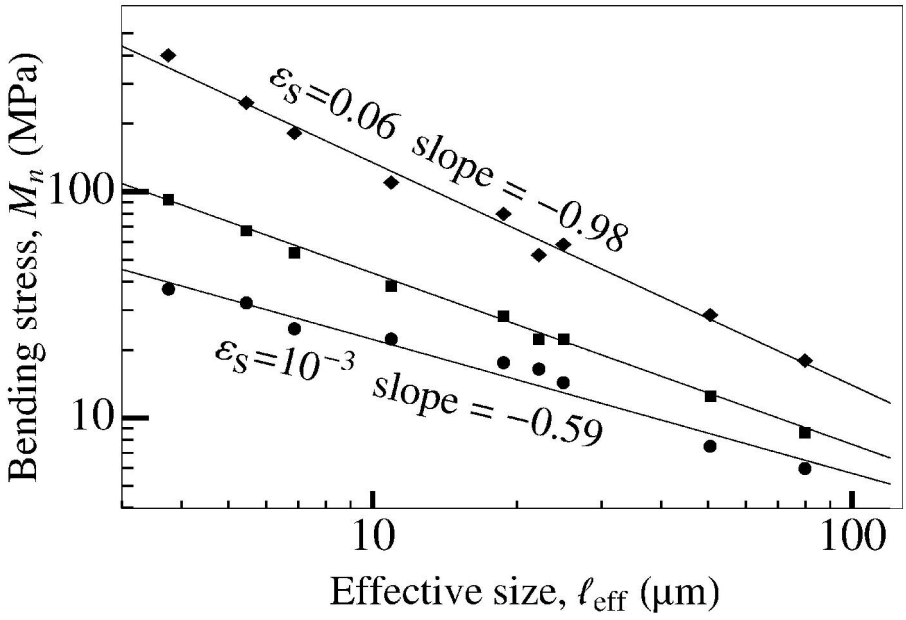

Figure 5
152x99mm (600 x 600 DPI)

Grain size and sample size interact to determine strength in soft metals. Supplementary on-line material

B. Ehrler, X.D. Hou, T.T. Zhu, K.M.Y. P'ng, C.J. Walker, A.J. Bushby and D.J. Dunstan

The data for three foils of thickness 10µm, 50µm and 125µm and grain size near 30µm are shown in Fig.2 of the main paper. To confirm the characterisation of the foils, we present some metallurgical images and a surface profile (Figs 1 to 4). For the convenience of workers who wish to use this data to test theoretical ideas, we tabulate below the strains and normalised bending moments (bending stresses) obtained for all nine combinations of thickness and grain size (Tables 1 to 9) together with the parameters obtained by fitting with eq.4 (Table 10)

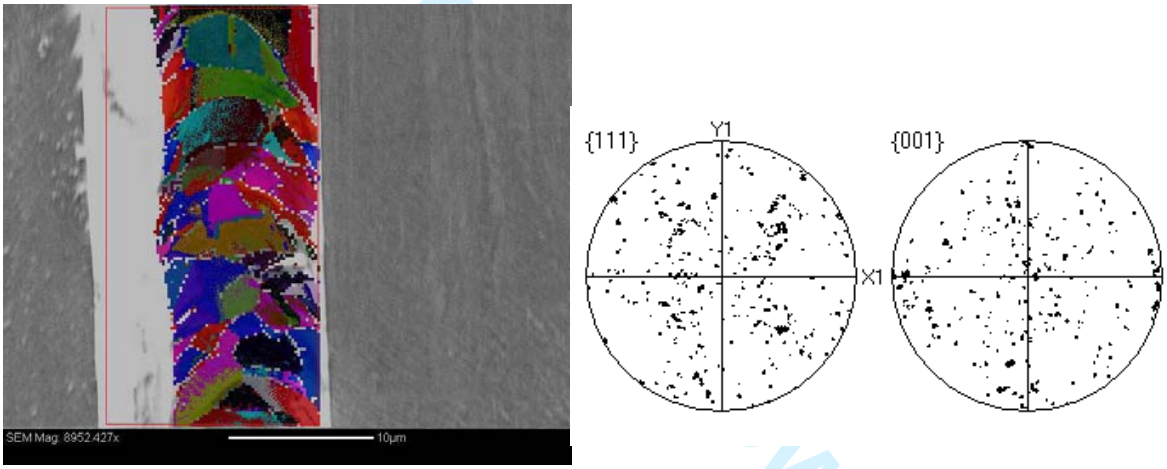

a **b**

Fig. S1 (a) An EBSD image obtained from the cross section of a 10 µm nickel foil, with grain size 6 µm shows equiaxed grains similar to those measured on the surface of the foil by the surface etch technique. **(b)** The EBSD pole figures illustrating the texture in the foil. The random texture confirms that grain orientation has little effect on the mechanical behaviour of the foils.

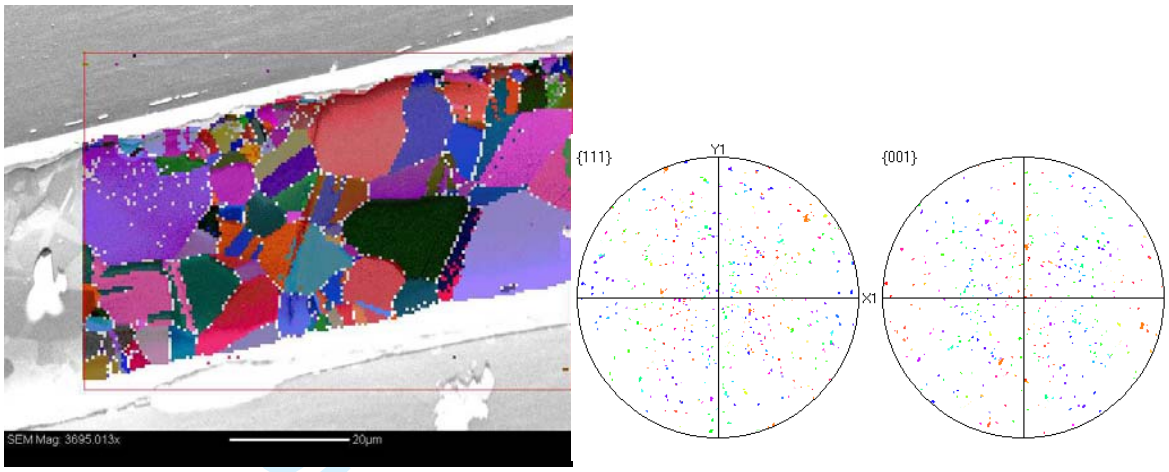

a **b**

Fig. S2. As Fig. S1, for a 50 µm foil with grain size 30 µm.

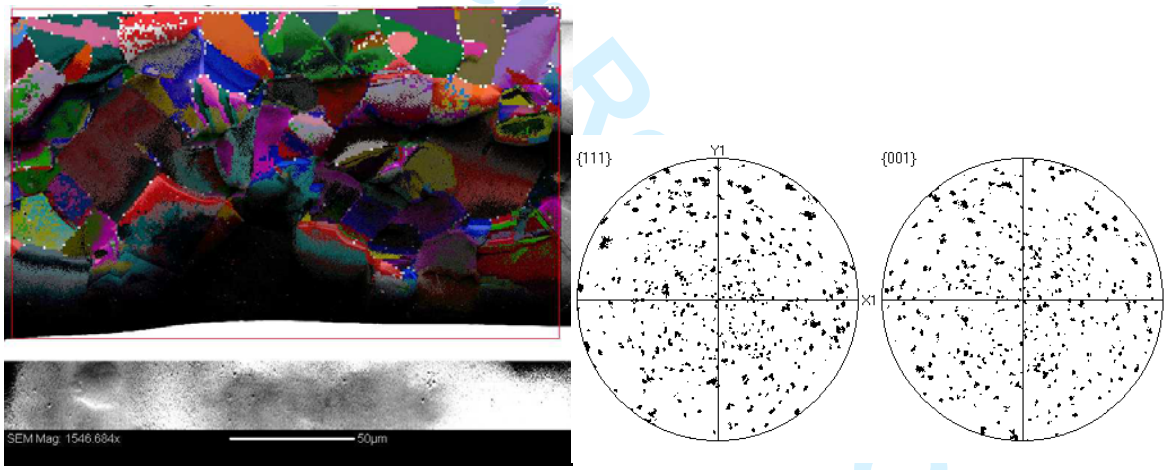

A **B**

Fig. S3. As Fig. S1, for a 125 µm foil with grain size 27 µm.

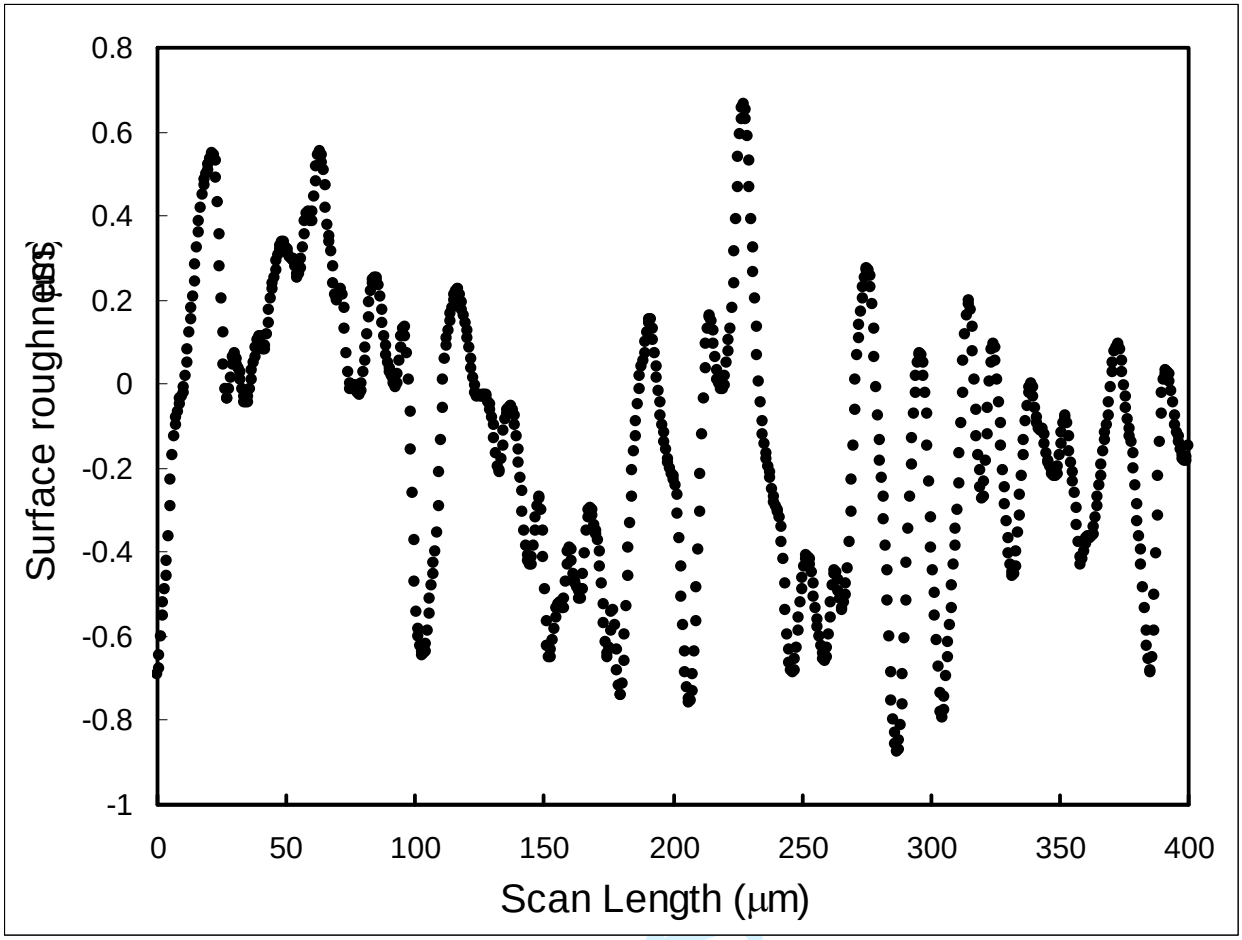

Fig. S4. Surface roughness, characterized by surface profilometry (using a Dektak 3ST). This profile is for a 50μm foil with grain size 14μm. The average roughnesses for all foils are given in Table S10 below.

Table S1: Foil thickness 10μm, grain size 6μm

Surface strain $\varepsilon_S = \frac{1}{2} h / R_1$	Normalized moment M_n from eq.1 (MPa)
0.00020	7.33
0.00035	12.8
0.00060	22.0
0.00085	31.2
0.00104	38.0
0.0050	61
0.010	91
0.030	217

Table S2: Foil thickness 10μm, grain size 12μm

Surface strain $\varepsilon_S = ½\, h / R_1$	Normalized moment M_n from eq. 1 (MPa)
0.00020	7.33
0.00035	12.8
0.00060	22.0
0.00085	31.2
0.0050	48
0.010	67
0.030	140

Table S3: Foil thickness 10μm, grain size 22μm

Surface strain $\varepsilon_S = ½\, h / R_1$	Normalized moment M_n from eq. 1 (MPa)
0.000012	0.42
0.000046	1.70
0.000085	2.90
0.000126	4.54
0.000143	4.94
0.000180	6.58
0.000208	7.62
0.000228	8.03
0.000261	9.13
0.000284	10.1
0.000316	11.3
0.000335	11.9
0.000336	12.3
0.000358	13.0
0.000374	13.3
0.000416	15.1
0.000441	16.2
0.000444	16.1
0.000461	16.6
0.000517	17.5
0.000638	19.0
0.000685	20.3
0.00072	20.9
0.00086	22.5
0.00091	23.0
0.00104	25.1
0.0050	35
0.010	53
0.030	108
0.045	147

Table S4: Foil thickness 50µm, grain size 14µm

Surface strain $\varepsilon_S = ½\, h / R_1$	Normalized moment M_n from eq. 1 (MPa)
0.000329	11.5
0.000360	12.6
0.000400	13.5
0.000443	14.8
0.000583	18.1
0.000700	19.4
0.000788	19.5
0.000867	20.7
0.001053	22.5
0.001262	22.4
0.001613	23.7
0.001896	24.2
0.025	63
0.050	98

Table S5: Foil thickness 50µm, grain size 30µm

Surface strain $\varepsilon_S = ½\, h / R_1$	Normalized moment M_n from eq. 1 (MPa)
0.000070	2.55
0.000179	5.97
0.000203	6.73
0.000231	8.24
0.000267	8.21
0.000320	10.1
0.000325	9.24
0.000389	11.7
0.000410	10.9
0.000472	12.9
0.000563	14.7
0.000578	13.0
0.000691	16.4
0.000746	13.9
0.000864	14.7
0.000916	17.6
0.000962	17.9
0.00103	16.9
0.00100	18.8
0.00115	18.5
0.00115	16.7
0.00120	19.0
0.00129	17.3
0.00178	19.6
0.00188	19.8
0.025	43

0.050	70

Table S6: Foil thickness 50μm, grain size 50μm

Surface strain $\varepsilon_S = ½\, h / R_1$	Normalized moment M_n from eq. 1 (MPa)
0.000333	8.88
0.000359	9.81
0.000447	11.4
0.000565	12.7
0.000586	12.2
0.000662	13.1
0.000982	14.1
0.00110	14.2
0.00125	14.4
0.00137	14.1
0.00153	15.7
0.00159	14.9
0.00185	15.7
0.00207	16.3
0.00227	15.9
0.025	34
0.050	52

Table S7: Foil thickness 125μm, grain size 27μm

Surface strain $\varepsilon_S = ½\, h / R_1$	Normalized moment M_n from eq. 1 (MPa)
0.000052	1.89
0.000243	6.56
0.000421	9.82
0.000500	11.6
0.000601	13.6
0.000751	14.9
0.000801	15.4
0.000919	16.1
0.00110	16.4
0.00781	20.6
0.0112	22.8
0.0136	24.7
0.0164	25.7
0.0179	28.6
0.0284	32.1
0.0588	52.4
0.050	47
0.036	36

Table S8: Foil thickness 125μm, grain size 85μm

Surface strain $\varepsilon_S = ½\, h / R_1$	Normalized moment M_n from eq. 1 (MPa)
0.000491	5.02
0.000660	5.96
0.000961	7.35
0.00154	7.94
0.00195	8.29
0.00237	8.79
0.00271	8.81
0.00322	9.72
0.00428	10.0
0.00515	10.6
0.0588	28.5
0.0357	21.5

Dataset 125.220:

Thickness 125µm
Grain size 220µm

Table S9: Foil thickness 125µm, grain size 220µm

Surface strain $\varepsilon_S = ½\, h / R_1$	Normalized moment M_n from eq. 1 (MPa)
0.000081	1.41
0.000206	3.57
0.000533	5.20
0.000924	5.73
0.001291	6.51
0.001550	5.80
0.001929	6.37
0.002800	6.90
0.003535	6.91
0.00411	7.04
0.0588	18
0.0357	15

Table S10: Fitting parameters using linear work-hardening (eq. 4)

Thickness (μm)	Grain size (μm)	Average surface roughness (μm)	Yield stress σ_0 (MPa)	Hardening rate k (MPa)
10	6	0.27	180	150
10	12	0.36	150	100
10	22	0.45	100	75
50	14	0.59	95	42
50	30	0.34	70	29
50	50	0.14	55	22
125	27	0.09	65	16.5
125	85	0.03	30	10
125	220	0.04	25	6